CrossMark

Flood risk assessment and mapping using AHP in arid and semiarid regions

Farid Radwan[1] · A. A. Alazba[1,2] · Amr Mossad[2,3]

Abstract

Identifying flood risk-prone areas in the regions of extreme aridity conditions is essential for mitigating flood risk and rainwater harvesting. Accordingly, the present work is addressed to the assessment of the flood risk depending on spatial analytic hierarchy process of the integration between both Remote Sensing Techniques (RST) and Geographic Information Systems (GIS). This integration results in enhancing the analysis with the savings of time and efforts. There are several remote sensing-based data used in conducting this research, including a digital elevation model with an accuracy of 30 m, spatial soil and geologic maps, historical daily rainfall records, and data on rainwater drainage systems. Five return periods (REPs) (2, 5, 10, 25, 50, 100, and 200 years) corresponding to flood hazards and vulnerability developments maps were applied via the weighted overlay technique. Although the results indicate lower rates of annual rainfall (53–71 mm from the southeast to the northwest), the city has been exposed to destructive flash floods. The flood risk categories for a 100-year REP were very high, high, medium, low, and very low with 17%, 41%, 33%, 8%, and 1% of total area, respectively. These classes correspond to residential zones and principal roads, which lead to catastrophic flash floods. These floods have caused socioeconomic losses, soil erosion, infrastructure damage, land degradation, vegetation loss, and submergence of cities, as well life loss. The results prove the GIS and RST effectiveness in mitigating flood risks and in helping decision makers in flood risk mitigation and rainwater harvesting.

Keywords Flood hazard · Flood vulnerability · Flood risk · GIS · RST · AHP

Introduction

Flash flood is a peak overflow of rainwater that generally appears during 6 hours of the outset of a torrential rainfall (Hoedjes et al. 2014; Starosolszky and Melder 2014; Deng et al. 2015; Archer and Fowler 2018). This flood happens in a very short time and has a considerable double effect. One results in the availability of an enormous amount of rainwater for different applications (Angelakis 2016; GhaffarianHoseini et al. 2016). The other is the enormous amount of water that leads to catastrophes and destruction (Abbas et al. 2016; Dale et al. 2016; Karagiorgos et al. 2016). These threats arise due to a deficiency of flood control systems to assimilate tremendous volumes of water during a storm. This enormous amount of water may involve different regions, including agricultural, industrial, and urban areas (Elfeki et al. 2017). Flash floods can entail both moral and material damages, including socioeconomic problems, destruction of the infrastructure, land and soil degradation, crop and vegetation damage, submergence of cities, and the loss of civilian life (Khan 2011; Mahmood and Mayo 2016; Mahmood and Ullah 2016; Ranjan 2017). Due to calamitous and devastating risks from flash floods, there is an imperious need for mitigating the impact of these floods. Hence, mapping the flood risks is crucial for mitigating these risks. The flood inundation and risk maps mainly depend on the hazard and vulnerability maps. Multi-Criteria Evaluation (MCE) is one of the approaches used to develop the hazards and vulnerability maps.

The MCE approach is widely used to assess flood risk. MCE plays a paramount role in deciding the best alternative

✉ Farid Radwan
  fradwan@ksu.edu.sa

1 Alamoudi Water Research Chair, King Saud University, Riyadh, Saudi Arabia

2 Agricultural Engineering Department, King Saud University, Riyadh, Saudi Arabia

3 Agricultural Engineering Department, Ain Shams University, Cairo, Egypt

for a precise purpose. This approach is based mainly on several factors. The MCE advantage is that it can be conducted efficiently to generate and rank all possible alternatives in conformity with their efficiencies. Therefore, the decision becomes a situational judgment between alternative solutions. Thus, the managers and planners can make their decisions based on one or more criteria. These criteria may either be factors or constraints. In general, factors are physically persistent in nature, including the slope gradient and road proximity factors. These factors can point to the relative relevance of certain regions. Otherwise, the selected restrictions or constraints are always of a logical nature, such as limitations due to reserved lands. Thus, these can serve to exclude particular territories from consideration. The MCE module can combine constraints and factors. The analytic hierarchy process (AHP) is the bestead method for implementing an MCE analysis, which was proposed by Saaty (1980). The AHP method permits carrying out the analysis through assessing, integrating, additionally ranking of the various conflicting factors at a certain degree of information. This method intends to choose an alternative solution. The participation rate for every criterion is identified. The suitable benchmark evaluation choosing is done drawing upon the defined relative weight of a collection of related rules. This process is conducted by comparing and judging the criteria in pairs, using the nine-point scale. In this comparison, the better criterion obtains a whole number on the Saaty scale from 1 (equal) to 9 (best). Meanwhile, the other criterion obtains the inverse of this value. Recently, there has been a considerable interest in using the AHP in natural hazard (e.g., earthquake and flood) assessment also besides in flood governance, where the flood risk can be assessed and mapped by AHP with reasonable accuracy. Flood risk is mapped using a weighted overlay tool in ArcGIS for hazard and vulnerability maps.

Flood hazard mapping based on AHP takes into consideration several criteria, like the runoff Curve Number (CN), drainage density, slope, and rainfall depth for judging flood event judiciously. The CN is representing the relationship between the Hydrologic Soil Groups (HSG) and Land Use/Land Cover (LULC) for a nominated area. CN value is ranging between 0 and 100, where 0 refers to high infiltration while 100 indicates high runoff (Gajbhiye et al. 2015; Li et al. 2015). The factors that influence CN are HSG, LULC, treatment, hydrologic condition, Antecedent Runoff Condition (ARC), and pervious and impervious areas (Mishra and Singh 2013; Ryu et al. 2016; Mahmoud and Gan 2018d). Natural Resources Conservation Service (NRCS) of the USA introduced the HSGs, where several diversified types of soil have been categorized by the soil specialist scientists into specified hydrologic soil groups (NRCS 2007) under the same physical features and runoff characteristics (Ibrahim-Bathis and Ahmed 2016). The key factors affecting the HSGs are the condition of the saturated hydraulic conductivity of the least transmissive layer, the soil depth above the impermeable layer, and water table depth.

Hydraulic conductivity has the upper hand between the above-mentioned factors (Lee et al. 2016). If these data cannot be obtained, the HSG is identified through a field survey. The data required during the field observations are soil texture, bulk density, soil structure strength, and water table depth. The NRCS had previously divided HSGs into four groups. However, three new dual groups have recently been introduced. The groups are A, B, C, D, A/D, B/D, and C/D (NRCS 2009). These groups are rated in descending order with respect to the infiltration rate. Group A refers to soils with high infiltrations rates (low potential runoff) and group D refers to soils with low infiltration rates (high potential runoff). Soil groups B and C refer to moderate and low infiltration rates, respectively (Shadeed and Almasri 2010; Ahmad et al. 2015; Mohammad and Adamowski 2015).

LULC describes the exploitation of a nominated area. The utilization may take several forms, such as water bodies, agricultural land, built-up land, barren land, and roads (Fisher et al. 2005). The classification process of these categories is intensive. Therefore, LULC classification is based on satellite imagery (Masoud 2016; Mack et al. 2017; Zhang et al. 2017), which can distinguish between LULC parameters. In this work, four LULC classes: roads, barren land, agricultural land, and urban were used. Subsequently, the CN value of every LULC class in every HSG conforms to the infiltration rate. Besides, the local temperature and rainfall are influenced by the land use changing (Mahmoud and Gan 2018a, b). The treatment describes the cultivation method used in agricultural lands, including tillage, terracing, hoeing, sowing, and contouring (Cronshey 1986). The hydrologic condition expresses the runoff or infiltration under different treatments and cover types (Gajbhiye et al. 2014). The three cases of hydrologic conditions, in descending order with respect to infiltration (Cronshey 1986), are good, fair, and poor. A good hydrologic condition generally refers to a high infiltration and low runoff. In contrast, the last hydrologic condition of the previous conditions has low infiltration and high runoff. ARC or pre-storm soil moisture has the lion's share of factors influencing the CN. ARC is representing the potential runoff index before the storm. The NRCS divides ARC into three cases: I, II, and III (Cronshey 1986), based on descending soil wetness (Oliveira et al. 2016). Thus, case I has dry soil but does not reach the wilting point. Since the NRCS estimates the values of CN based mainly on case II (Sartori et al. 2011), the same case has been applied in this work. However, the values of CN should be adjusted considering cases I and III as well. The CN value changes depending on connected or unconnected impervious areas. If the impervious areas are attached directly to

the system of storm drainage, the water will not be lost by infiltration (Cronshey 1986).

Drainage density is the greatest important morphometric parameters. It reveals the impact of terrain, LULC, and soil texture in the watershed area. Drainage density is a proportion of the total length of stream portions in the watershed to the area of the watershed, expressed as km/km^2 (Horton 1932; Avcioglu et al. 2017; Wu et al. 2017; Yalcin and Gul 2017). Many factors influence drainage density, which controls the characteristic length of the basin. These factors include landscape dissection features related to drainage density such as the soil texture, rock characteristics, vegetation, climate, and relief (Abboud and Nofal 2017; Rai et al. 2017). Low drainage density values indicate a highly permeable sub-soil, thick vegetation cover, and low-to-moderate relief (Abdelkareem 2017; Ghorbani Nejad et al. 2017; Radwan et al. 2017). In contrast, high drainage density values indicate that there are impermeable subsurface materials, mountainous reliefs, and sparse vegetation (Benzougagh et al. 2017; Redwan and Rammlmair 2017). In general, drainage density increases with decreasing infiltration capacity or transmissivity of the soil.

The slope is an inclination of the Earth from an imaginary horizontal plane (Rimba et al. 2017). It depends essentially on the terrain lithology nature, structure, soil, vegetation, climate, landforms, and morphogenetic processes which forming the underlying rocks. The Climate Forecast System Reanalysis (CFSR) daily precipitation data records, acquired from the National Centers for Environmental Prediction (NCEP), were employed in this research. Several studies employed these precipitation records to name a few (Dile and Srinivasan 2014; Fuka et al. 2014; Mohan and Rajeevan 2017; Tirkey et al. 2017). The CFSR daily data for 36 years (1979–2014) was used for frequency analysis. These analyses are mainly aiming to estimate a specific precipitation event probability that will equal or exceed in any particular year. The precipitation recurrence intervals depend mainly on the storm event duration and magnitude, whereas streamflow recurrence intervals are contingent entirely upon the anniversary peak flow magnitude. The utilized return periods (REPs) (2, 5, 10, 25, 50, 100, and 200 years) in this research were depending on a Log Pearson III distribution. This distribution type is best appropriate for hydrological analysis (Subyani and Al-Amri 2015; Amin et al. 2016), and this prediction enables the alleviation of flood risk-prone areas at any future time.

Flood vulnerability mapping based on AHP uses three criteria: LULC, the system of storm drainage, and demographic data such as population density (Danumah et al. 2016). These data form essential pillars in flood risk mitigation. The storm drainage system expresses the water volume that the system can accommodate. Urbanization influences hydrological characteristics such as increasing runoff, decreasing infiltration, and increasing flood depth and frequency. Meanwhile, population density expresses the total number of people in a specific region. A continuously growing population with decreasing agricultural lands leads to increased flood risks in the future. Therefore, urban areas suffer from high flood risk due to their high census, land use properties, and infrastructure. Several studies have integrated mapping and assessing flood risk (Stefanidis and Stathis 2013; Ouma and Tateishi 2014; Papaioannou et al. 2015; Rahmati et al. 2016).

Therefore, the present study assesses and maps flood risk for arid and semiarid regions based on spatial AHP and Geographic Information Systems (GIS) integration in order to introduce a unique tool to help decision makers in mitigating flood risk and harvesting rainwater. The underlying merits of this methodology are simplicity and low cost.

Description of the study area

Riyadh city (latitude 24°13′51″N to 25°10′30″N and longitude 45°59′12″E to 47°20′29″E) is the capital of the Kingdom of Saudi Arabia (Fig. 1). While the Riyadh metropolitan area is 6570 km^2, the watershed area is 8500 km^2. The Riyadh city was selected as a perfect location for conducting this case study because it is a large cosmopolitan city with a huge infrastructure supported by agricultural and industrial sectors. Moreover, it is considered one of the world's fastest expanding cities with a population of 6.5 million (Aina et al. 2008; Ashwan et al. 2012; Mahmoud and Gan 2019). Furthermore, the soil texture of Riyadh is varied, including sand, loam, and gravel. The ordinary city climate features a hot-dry summer, and a cool-moist winter. The average temperature is highest (22–43 °C) from June to August and lowest (8–22 °C) from December to February (Qhtani and Al Fassam 2011). Despite a deficient annual average precipitation of about 62 mm, the city periodically experiences flash floods (Rahman et al. 2016; Mahmoud and Gan 2018c). However, lately, a change in the precipitation style has resulted in continuous downpours, causing a high volume of surface runoff. This flooding leads to socioeconomic loss, soil erosion, destruction of infrastructure, land degradation, vegetation loss, the inundation of cities, and loss of life (Bajabaa et al. 2014; Špitalar et al. 2014).

Methodology

Flood risk assessment plays an indispensable role in flood risk mitigation and rainwater harvesting. The MCE using AHP in a GIS ambience is one of the several approaches used for mapping flood risk. The methodology of mapping the flood risk has been divided into two main steps,

Fig. 1 Location map of the Riyadh metropolitan area
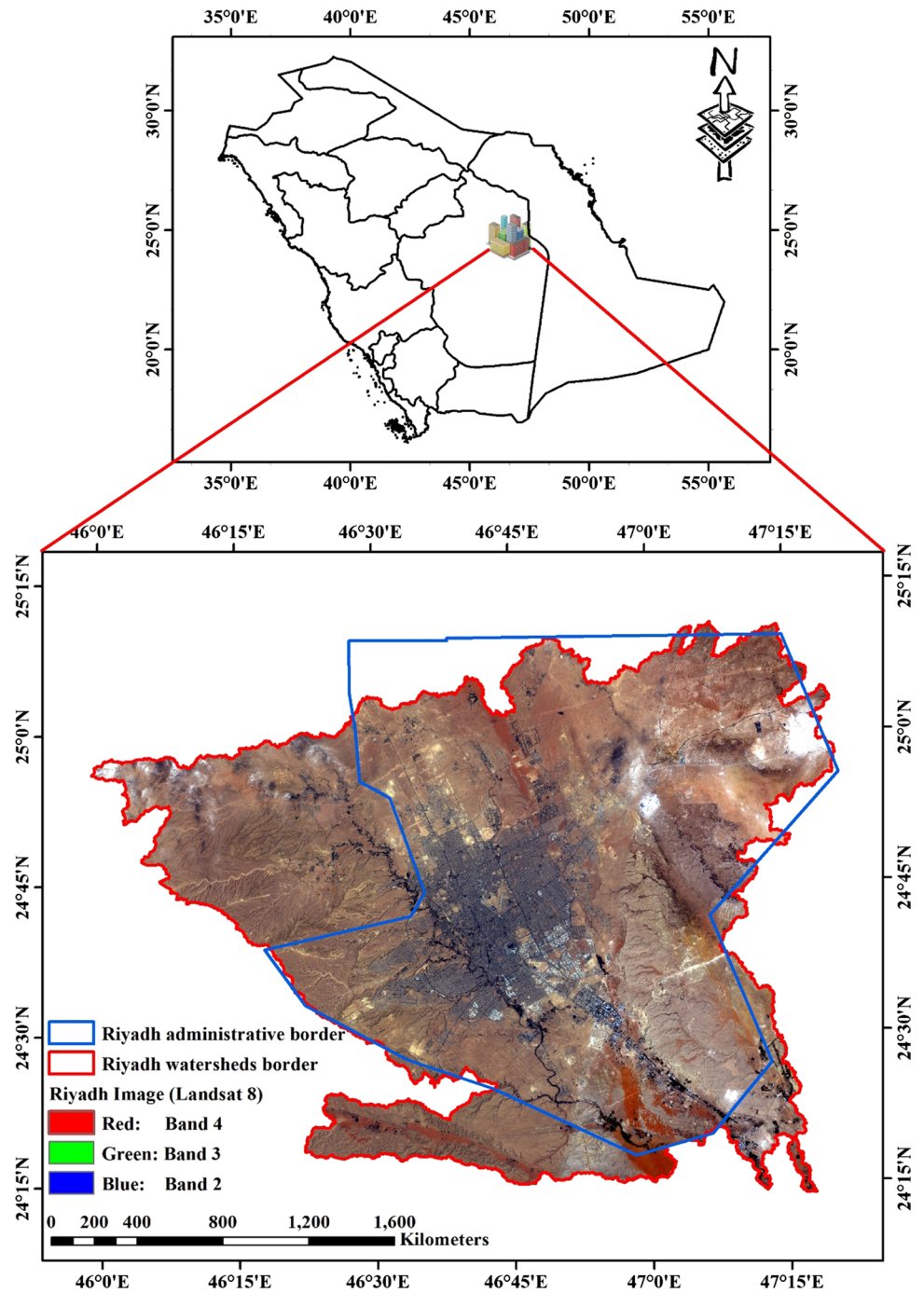
as shown in Fig. 2. The two steps of this methodology are creating spatial maps of the flood hazard and vulnerability. The parameters required for the development of each of these maps are the digital elevation model (DEM), soil map, geologic map, satellite imagery, daily precipitation records, population density and detailed information on the present rain storm drainage for Riyadh city. Table 1 contains all the data along with their sources. The World Geodetic System 1984 Universal Transverse Mercator (WGS 84 UTM) with coordinate reference system of zone 38 was used as the geographic projection system in all the developed maps.

The first step in this methodology for the development of flood risk maps was creating the flood hazard maps. Subsequently, the determination of the hazard employed several parameters over the study area, including drainage density, CN, slope, and precipitation. The source of a 30 m DEM (Fig. 3) was the United States Geographical Survey (USGS). This USGS-DEM was the basis in developing the spatial map of the drainage density through the following steps:
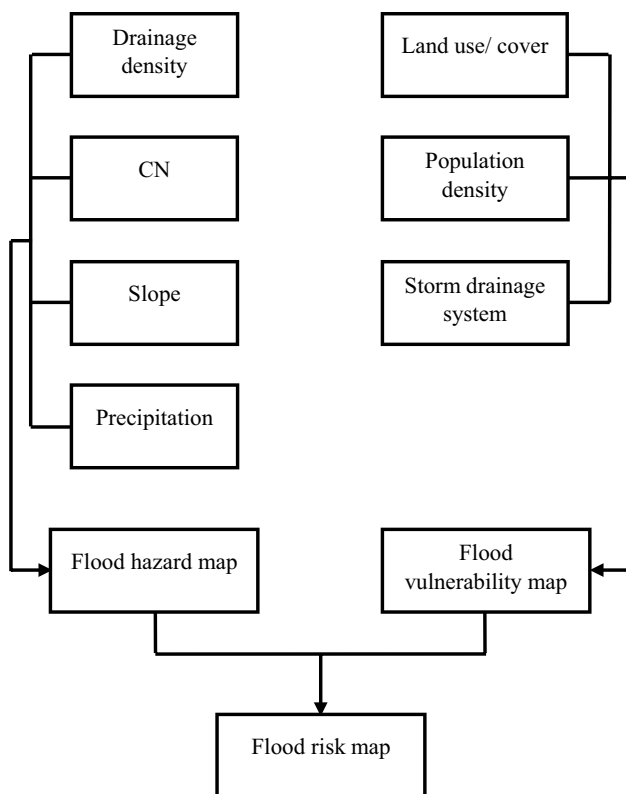
Fig. 2 Applied GIS-based for mapping flood risk in the study area

Fig. 3 Digital elevation model (DEM) of the study area

Table 1 Data used with their sources

Data	Data type	Data sources
DEM	1 Arc, 30 m	USGS
Satellite image	Raster, 30 m	USGS
Soil map	JPEG image	MEWA
Geologic map	JPEG image	SGS
Precipitation	Daily records	CFSR
Population density	Records	GaStat
Storm drainage system	JPEG image	Riyadh Municipality

The year of use for all data is 2017

filling the DEM, determining flow direction, flow accumulation and conditions, and calculating the total stream length, including total basin area. The map of slopes was derived by default from the USGS-DEM during the analysis process.

The CN values were mapped by amalgamating the HSG with LULC. The HSG was developed from the spatial maps of the soil texture and geologic. The data source for the soil texture and geologic maps is the Saudi Ministry of Environment, Water, and Agriculture (MEWA) and the Saudi Geology Survey (SGS), respectively. Both maps were downloaded as images and then processed to get the final form of those maps as follows: giving geo-referenced information,
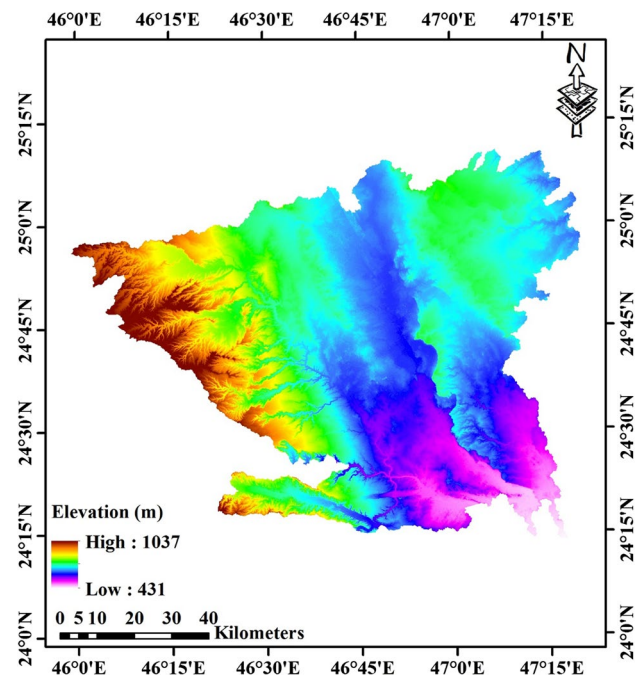
digitizing, reclassifying, and clipping the map for the borders of the watershed. Eventually, the HSG map has been prepared by incorporating the available information from geologic and soil texture maps.

The Riyadh metropolitan area LULC map was generated employing satellite images from Landsat 8 (Fig. 1). These images have a resolution of 30 m and were obtained from the USGS. The image was first classified using unsupervised and supervised classifications. Both classifications were accomplished employing ENVI 5.3. The supervised classification of the LULC was divided into four classes: urban, barren land, agricultural land, and roads. The LULC map was based on supervised classification as it can accurately distinguish the land features of the study area as compared to unsupervised classification. Additionally, the CN was estimated for every cell by using the combination tool in ArcGIS 10.4. Thus, these computations were based on the CN values for LULC and HSG under ARC II conditions (Table 2). Consequently, the map of CN values was generated by mainstreaming the HSG map and the LULC map.

The precipitation distribution of the entire study area was mapped by using daily rainfall records from the CFSR data. The interpolation applied to the data of 24 meteorological stations from 1979 to 2014 (36 years) is the isohyetal method. The REPs considered in this work to anticipate any eventual annual precipitation recurrence were 2, 5, 10, 25, 50, 100, and 200 years. The daily precipitation data frequency analysis is based on the distribution of log Pearson type III (as best distribution for hydrologic data), using

Table 2 Curve Number (CN) values for Land Use/Land Cover (LULC) and Hydrologic Soil Group (HSG) under Antecedent Runoff Condition (ARC) II case

Land use/cover	Hydrologic soil group			
	A	B	C	D
Urban	89	92	94	95
Barren land	77	86	91	94
Agricultural land	64	74	81	85
Road	98	98	98	98

Table 3 Random index (R_I) values (Saaty 1980)

Number of criteria	R_I
2	0.00
3	0.58
4	0.90
5	1.12
6	1.24
7	1.32
8	1.41
9	1.45
10	1.49
11	1.51

hydrological frequency analysis (HYFRAN) software. The frequency analysis values help in the appreciation of potential runoff depth at any time in future. Subsequently, decision makers can assess reduction in flood risk with prudent watershed management. In the end, a hazard map was created from the amalgamation of those data discussed above.

The second step in developing flood risk maps was creating the flood vulnerability map. The inputs data for this step were LULC map, population density, and the storm drainage system. The data source for population and drainage system is the Saudi General Authority for Statistics (GaStat) and the Riyadh city municipality, respectively. Thereafter, the population density maps and the storm drainage system were interpolated and cropped for the watershed borders. Then, the vulnerability map was generated by integrating the data, as mentioned earlier.

Identify the sharing effect rate of each considered criterion in the risk locations determination was based on the AHP. It is based on the pairwise comparisons respecting the weighted. There were six levels in this process: outlining the problem, building the AHP hierarchy, creating the pairwise comparison matrix, identifying every criterion value to compute the criteria weights, checking the acceptance of consistency ratio, and ranking the available alternatives. The pairwise comparison is the key ingredient of the AHP. Every criterion was compared with the other criteria under the same option. The suitable criterion in this comparison takes an integer number according to the Saaty scale, which ranges from 1 (equal) to 9 (best). Meanwhile, the other criterion in the comparison receives the inverse of this value.

Developing the matrix for the AHP options required several steps. The first step of AHP matrix development was determining the criteria eigenvectors (Vp) through (Eq. 1).

$$V_p = \sqrt[k]{W_1 \times W_2 \times \cdots \times W_k} \tag{1}$$

where k is the number of compared parameters, and W_1 and W_k are the weight of criterion 1 and k, respectively.

The second step in the AHP matrix development was finding the weighting coefficient (C_p). One of the most important rules that must be taken into consideration is that the total of

the C_p is equal to one. The following equation was applied to calculate the C_p:

$$C_p = \frac{V_p}{V_{p1} + V_{p2} + \cdots + V_{pk}} \tag{2}$$

The third step involved computing the eigenvalue (λ_{max}) with the following equation:

$$\lambda_{max} = \frac{[E]}{k} \tag{3}$$

where $[E]$ is the rational priority which can be determined as follows:

$$[E] = \frac{\sum \text{ of row of normalization matrix}}{C_p} \tag{4}$$

The created matrix was normalized by dividing each component of the column by the summation of the column.

In the fourth step, the consistency index (C_I) was computed as per the following equation:

$$C_I = \frac{(\lambda_{max} - k)}{(k - 1)} \tag{5}$$

The fifth step was determining the consistency ratio (C_R) using (Eq. 6). It takes into account that this ratio does not exceed 10%, as proposed by Saaty (1980). The weights were reviewed several times until the C_R reached the required value.

$$C_R = \frac{C_I}{R_I} \tag{6}$$

where R_I is an index of random values recommended by Saaty (1980). These values are mentioned in Table 3.

Finally, the following equation was used to determine the hazard and vulnerability indexes.

$$\text{Option index(Hazard or Vulnerability)} = \sum V_p \cdot C_p \tag{7}$$

The flood risk map in this study was created through the weighted overlay tools incorporated in the GIS environment as this tool allows integrating both hazard and vulnerability maps, in accordance with the following equation:

$$\text{Risk} = \text{Hazard} \times \text{Vulnerability} \tag{8}$$

Results and discussion

Earlier, flood-prone areas were assessed by employing the hydrologic/hydraulic models that depend fundamentally on water flow balance and waterways conveyance. However, an unconventional technique for identifying the prospective flood risk areas, which incorporates the hazard and vulnerability maps of the flood, has been adopted in this project. The hazard and vulnerability locations in the city were defined in two stages. The first stage involved selecting the flood-causative criteria. The sharing rate of each criterion was defined in the second stage. A multi-criteria approach (AHP-based) was used to explain the inconveniences linked to the overabundance of water during inundation events. The AHP method, with the integration of GIS, has been preferred by several studies (Stefanidis and Stathis 2013; Ouma and Tateishi 2014; Danumah et al. 2016; Rahmati et al. 2016). Therefore, the present study tried introducing a realistic solution for the flood risk criteria in the ungauged area under extreme conditions using AHP. This approach has a higher accuracy than traditional methods that depend on hydraulic-only models.

The AHP method is important as it facilitates the analysis and organization of such complex systems while taking into consideration several dimensions (features of situations) of the MCE in a more significant way. These features of situations considered in this work are based fundamentally on the CN as an empirical parameter for direct runoff prediction, drainage density, slope, precipitation rate, LULC, population density, and the system storm drainage. Several difficulties were observed during this project to name a few, the data deficiency as well as the fact that the acquired data were retrieved from several sources with different specifications (e.g., different acquisition dates for the satellite images, several formats, and different resolutions). These issues have not limited the work quality due to employing the weighted ranking for the flash flood factors under the AHP-based.

Hazard map

The flood hazard, similar to a natural disaster, is difficult to manage due to several factors influencing it. The hazard caused by a flood indicates the presence of an extreme hydro-climatic event with abundant flowing water. The flood hazard was mapped by combing the related factors (e.g., CN, drainage density, slope, and precipitation). Figure 4
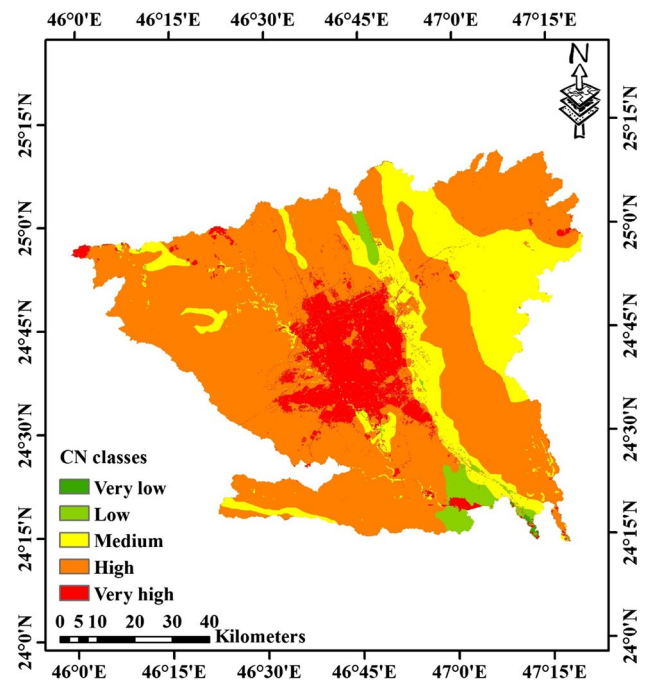

Fig. 4 Curve number (CN) map for the entire city

shows the entire city CN values, which ranged from 64 to 98, and have been categorized as five classes (very high, high, medium, low, and very low). The highest land percentage was covered by the CN classification of high and medium with 66% and 20.5%, respectively. Meanwhile, the rest classes, very high, low, and very low had a land percentage of 11%, 2.4%, and 0.1%, respectively. Hence, about 80% of the overall city area had CN values above 90. The highest CN values indicate the existence of urban land, barren land, and roads while the moderate CN values refer to the agricultural lands. The value of the average weighted CN for the studied area was 92. These CN values emphasize that the project area has many places have high impermeable zones distinguished by the general physical characteristics of rocks (decreasing infiltration rates). Moreover, the area has no or little vegetation cover which also leads the runoff rates to increase.

The drainage density of an area affected by soil type and LULC. Figure 5 shows a drainage density of 2.61 km/km². This map is classified into five classes of drainage density: very high, high, medium, low, and very low. The classes percentages area were 31%, 28.8%, 18%, 15.5%, and 6.7% for low, medium, high, very low, and very high, respectively. It is worth noting that the high and very high drainage densities were found in urban areas, agricultural lands, and main roads while the low and very low drainage densities were found in areas that have a lacking vegetation. The higher drainage density values refer to the continuation of impermeable subsurface materials, high reliefs, and/or sparse
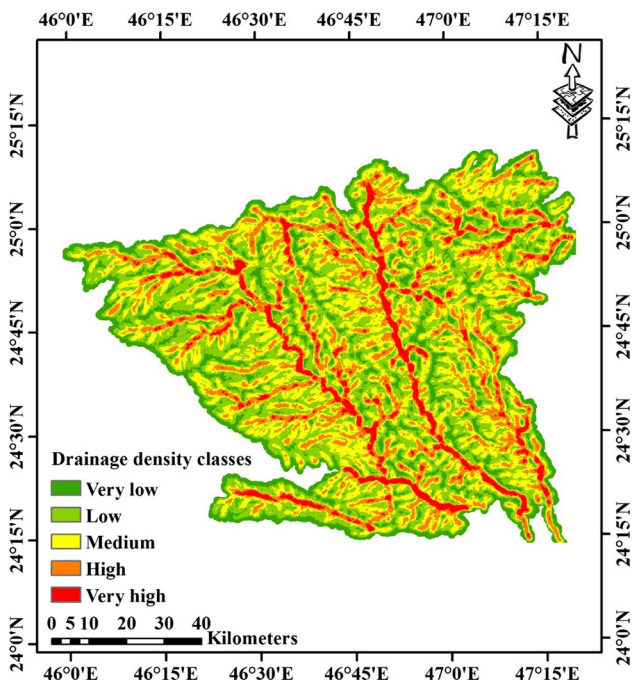
Fig. 5 Drainage density map of the study area

vegetation. In other words, a high drainage density causes high runoff rates.

The study area slope varies from 0° to 52°. Figure 6 depicts the study area slope classes, which are categorized into five main classes as very low (< 2.5°), low (2.5°–6.5°),
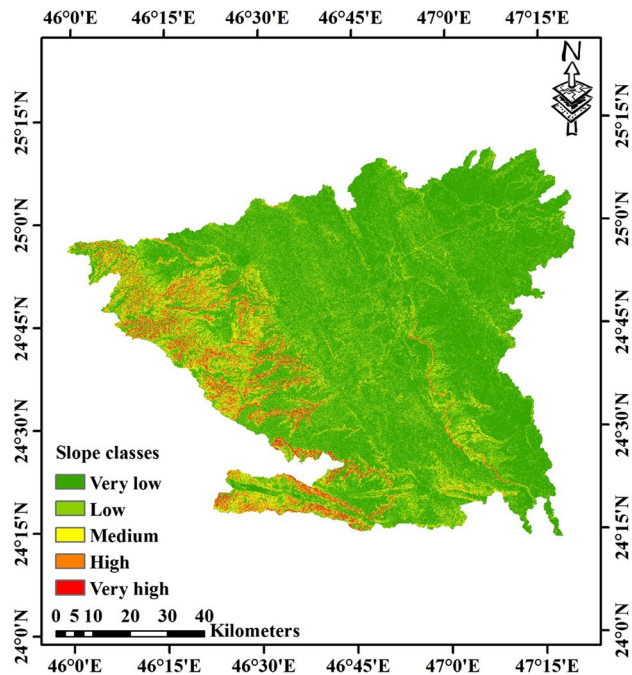
medium (> 6.5°–12.5°), high (> 12.5°–20°), and very high (> 20). Each class occupies a percentage of 59%, 28%, 7%, 4%, and 2% of the studied area, respectively. It is worth noting that the city is sloped from the south to the southeast. The maximum difference in the slope was found in the western portion of the research area. This provides another illustration of the terrain nature with regard to runoff and infiltration. Thus, any slight slope might result in more areas getting affected by extreme inundation events.

It is estimated that the annual average precipitation would range between 53 and 71 mm during the considered time scale of the precipitation data. This amount of rainwater would mainly fall from the southeast to northwest. As illustrated in the preceding sections of this article, with all the other factors affecting the flood hazard, the precipitation rates were classified into five classes. Figure 7 shows these precipitation classes, which are very low (< 56 mm), low (> 56–59 mm), medium (> 59–62 mm), high (> 62–65 mm), and very high (> 65 mm). Each precipitation class covers 18%, 20%, 23%, 25%, and 14%, respectively, of the study area. Rainwater more than 60 mm covers the city barren regions, where it extends widely throughout the northern and northwestern regions. The rainwater depths ranging between 55 and 60 mm were concentrated in the city center. These intensive precipitation rates create a considerable chance of causing a flash flood.

The proposed weights should be suitable for developing a flood map with hazard levels using the AHP method. The proper weights requirement is fulfilled whenever the
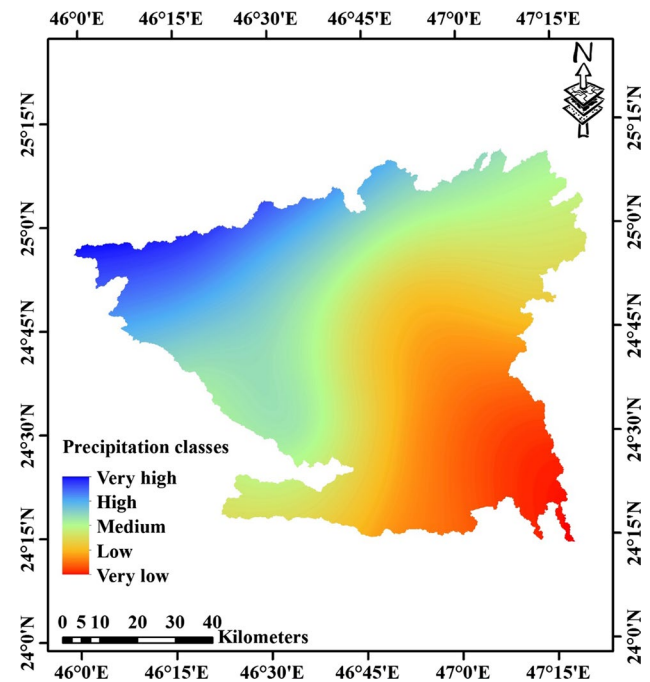

Fig. 6 Slope map of the study area

Fig. 7 Annual average precipitation distribution map of the study area

Table 4 Hazard matrix

	Dd	CN	Sp	Prec.	V_p	C_p
Dd	1	3	1/3	1/5	0.67	0.14
CN	1/3	1	1/3	1/5	0.39	0.08
Sp	3	3	1	1/3	1.32	0.24
Prec.	5	5	3	1	2.94	0.54
$\sum$	9.33	12	4.67	1.73	5.32	1

Table 5 Normalization of hazard matrix

	Dd	CN	Sp	Prec.	$\sum$ of rows	[E]	λ_{max}	C_I	C_R
Dd	0.11	0.25	0.07	0.12	0.54	4.08	4.204	0.068	0.08
CN	0.04	0.08	0.07	0.12	0.31	4.08			
Sp	0.32	0.25	0.21	0.19	0.98	4.35			
Prec.	0.54	0.42	0.64	0.58	2.17	4.31			
$\sum$	1	1	1	1	4	16.82			
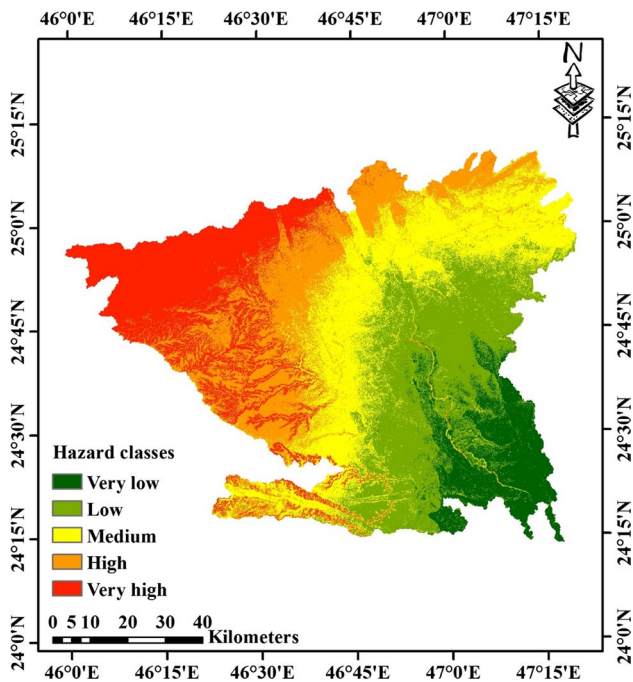
Fig. 8 Hazard map for every cell of the study area

consistency ratio is under 10%. Table 4 presents the weighting coefficients with their eigenvectors for all the criteria applied in this work. The weighting coefficients percentages were 14%, 8%, 24%, and 54% for drainage density, CN, slope, and precipitation, respectively. Table 5 provides the eigenvalue, consistency index, and consistency ratios of these criteria. Since the C_R of the hazard matrix was about 8%, the weights can be regarded as suitable for creating the hazard map.

Figure 8 provides the hazard map for the entire city. This map illustrates the potential areas liable to flash flood events.

As shown in this map, the hazard levels were grouped into five classes: very low (covering 10% of the area), low (24%), medium (25%), high (22%), and very high (19%). Additionally, the hazard levels of very low, low, and medium were found to appear over barren lands and roads. These typically are areas with steep slopes as well as low values of CN, drainage density, and rainfall. The high and very high levels of hazard were evident in the agricultural lands and urban areas. Thus, these areas are often characterized by gentle slopes in addition, the high values of CN, drainage density, and precipitation. Overall, a high hazard value indicates high risk.

Vulnerability map

The vulnerability map provides fine-tuned information about the potential flash flood-prone areas. The factors affecting the vulnerability can be summarized in socioeconomic activities such as people with their economic interests that may be affected by any natural hazard phenomena in terms of quantity and quality (Danumah et al. 2016). In other words, the vulnerability map is the combination of factors like the LULC, population density, and storm drainage system. Hence, every factor should be weighted through the AHP method to identify these weights. Within the above-mentioned factors, LULC has the upper hand in runoff and flood behavior determination. Accordingly, both the unsupervised and supervised classifications were deployed for the land-cover assessment. Figure 9 shows the unsupervised land-cover classes map. Although this map is divided into six classes, some of the land features did not appear in these classes (e.g., road layer). Thus, the unsupervised land-cover map showed no clear evidence of some of the land features.

On the contrary, the supervised map could provide more details of the land cover. The supervised land-cover map is
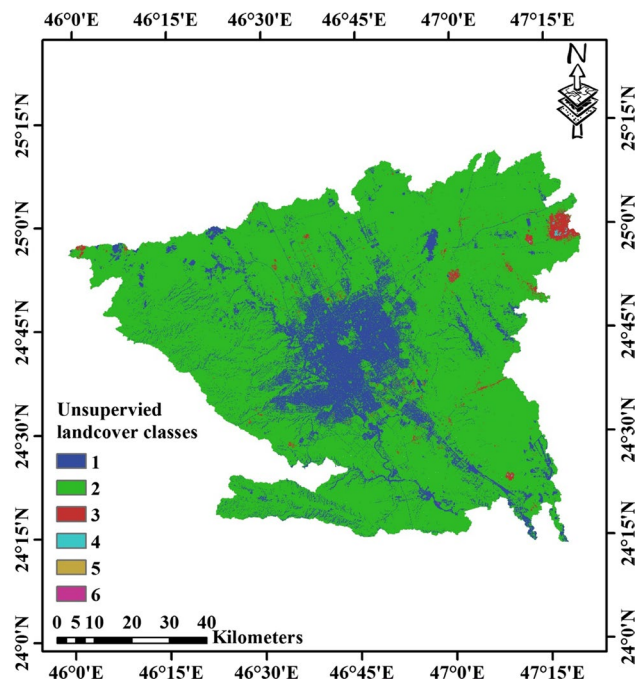
Fig. 9 Unsupervised land cover map of the study area

shown in Fig. 10. This figure confirms that the Riyadh land-cover map consists of four land feature classes. These classes are roads, urban zones, agricultural lands, and barren lands. As also exemplified from the supervised land-cover map that upwards of 87.9% of the city was covered by barren land.
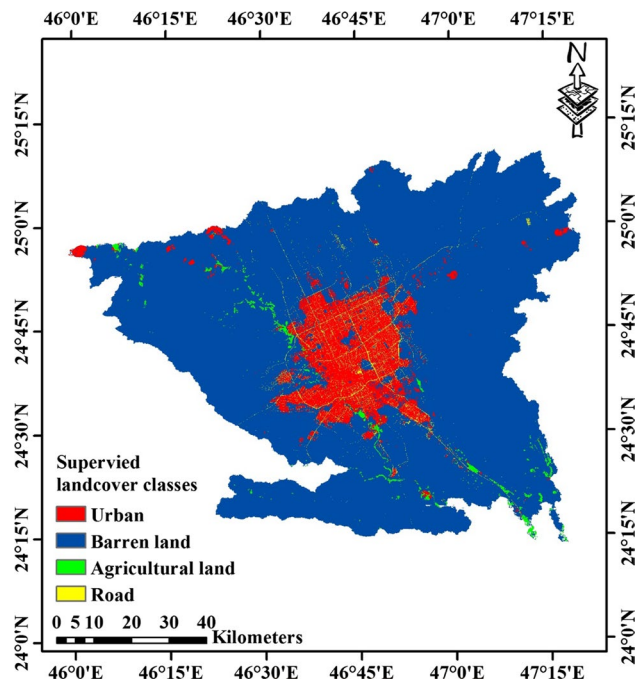
The total land-cover percentages areas were 9.0%, 1.5%, and 1.6% for urban, agricultural, and roads, respectively. Additionally, the barren lands are located on the outskirts of the city while the rest classes of the land cover are situated in the center. There are many other circumstances that may increase the damaging effects of the flash flood (e.g., unplanned urbanization expansions, impermeable areas like asphalt, and lack of vegetation). Consequently, these conditions lead to flash flood risks rising in the Riyadh metropolitan area.

One of the instrumental components of flash floods vulnerability determination is the population density distribution map. Therefore, this spatial distribution map was produced by interpolating the GaStat census data. Figure 11 depicts the population density classes map (very low, low, medium, high, and very high) with the percentage of the total city area as 25%, 15.5%, 26%, 19%, and 14.5%, respectively. It was observed that the classes of high and very high population density were in the city's middle, which was mainly covered by agricultural and urban lands and the low and very low population density classes were found at the city suburbs with barren land and deserts. There is a direct correlation between the high population density and extreme vulnerability. It is interesting, however, that people with sufficient experience in dealing with risks have fewer problems than others (Ruin et al. 2008, 2009; Špitalar et al. 2014). In this regard, none of the Asians died from the flash flood events in Saudi Arabia (Rahman et al. 2016).
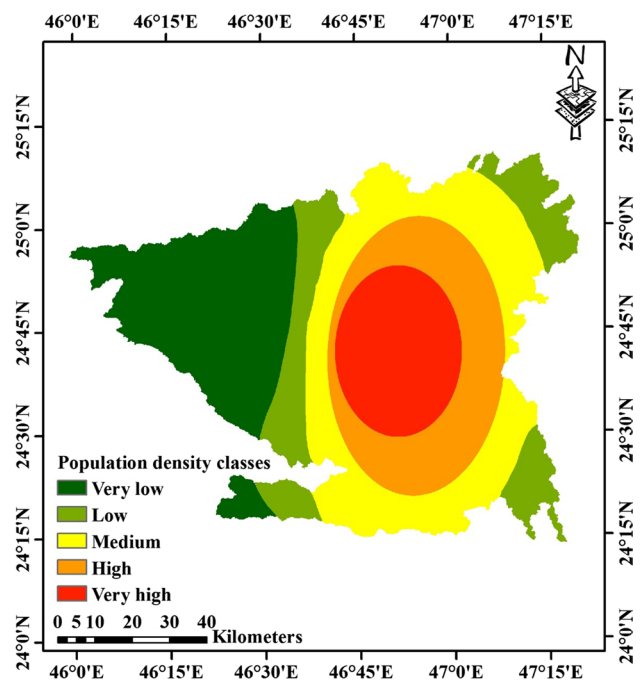

Fig. 10 Supervised land-cover map of the study area

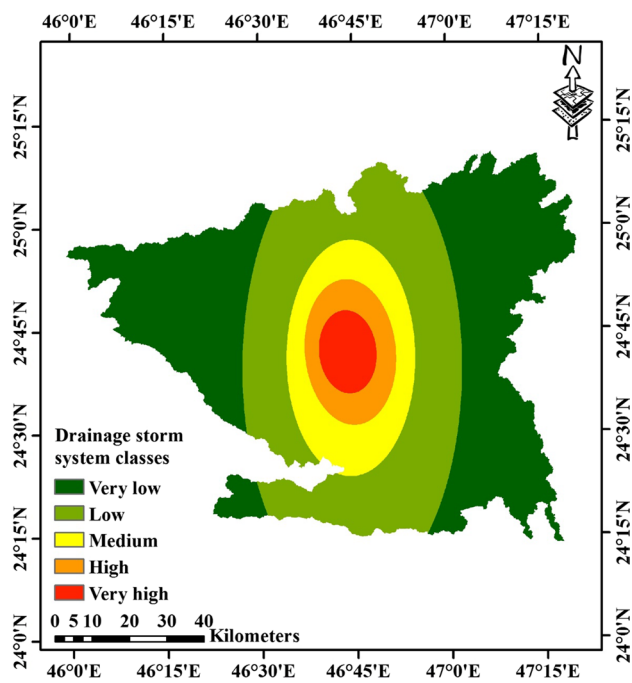**Fig. 11** Population density distribution map of the study area

Fig. 12 Drainage storm system map of the study area

The storm drainage system distribution over the study area was spatially mapped by interpolating the data of the storm drainage network. Figure 12 shows the storm drainage system classes. There are five classes, based on the drainage networks availability. These classes are very low, low, medium, high, and very high, covering 45.5%, 34%, 11%, 6%, and 3.5% of the total research area, respectively. The classes of very high, high, and medium storm drainage systems are situated in the midtown where the infrastructure is well constructed. Contrarily, the low and very low storm drainage systems were stationed in the suburbs of the city with the low population densities.

There is a clear link between the population density and the extreme flash flood events vulnerability. In other words, the high population densities areas cannot be affected greatly by the flash flood if there are the effective systems of the storm drainage to protect these vulnerable areas. Thus, this study can help the municipality planners in identifying the system capacity of the storm drainage adequately with a view to ensuring accommodating the water volumes of flash flooding.

Since weighted factors are necessary for mapping the vulnerability using the AHP, the weighting and eigenvectors coefficient were calculated for all vulnerability criteria. Table 6 provides these values. The weighting coefficients of LULC, population density, and storm drainage system were 26%, 63%, and 11%, respectively. Table 7 gives the eigenvalue, consistency ratio, and consistency index of the vulnerability map. Since the C_R is about 3%, the weights

Table 6 Vulnerability matrix

	LULC	Pop.	DS	V_p	C_p
LULC	1	1/3	3	1.00	0.26
Pop.	3	1	5	2.47	0.63
DS	1/3	1/5	1	0.41	0.11
Σ	4.33	1.53	9.00	3.88	1

can be regarded as suitable for the vulnerability map accomplishment.

Figure 13 shows classified the city vulnerability map into five classes. These classes are very low, low, medium, high, and very high, covering about 25%, 15%, 26%, 19%, and 15% of the total area, respectively. Barren lands had a low and very low level of flash floods vulnerability level. This is ascribed to the low and very low population densities with low and medium systems of storm drainage. However, agricultural land, urban land, and roads have medium, high, and very high flash floods vulnerability, respectively. These areas also have a high and very high level of population density and the system of storm drainage. In general, high vulnerability refers to high risk.
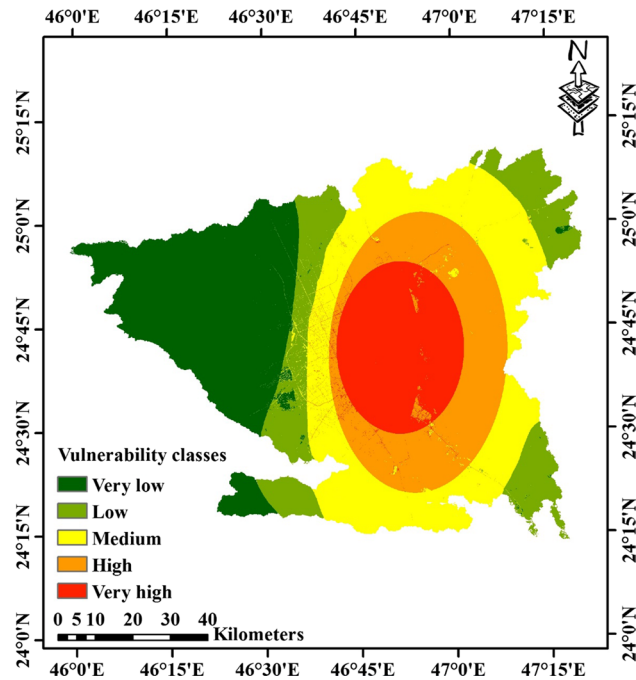
Risk map

The spatial flood risk map is essentially an integration between the hazard and vulnerability maps prepared according to the AHP method. Figure 14 depicts the flash flood risk map, which is divided into five classes (very low, low, medium, high, and very high), developed in this study. Each flood risk class is found for every cell in the city at different REPs. Accordingly, the high and very high flood risks were observed in the urban zones and roads of the city. The medium risk level was observed for land covers such as agricultural, barren, and urban zones. The low and very low risks were noticed in the barren land on the city outskirts. The presence of low and very low risks sites can be traced back to the existence of permeable soils, steeper slope, very low census, and low drainage density.

Table 8 presents the percentage area that is covered by the various risk classes at different REPs. For 2- and 5-year REPs, low and very low risks were found in the city. For 10- and 25-year REPs, the medium risk areas began to increase, and the low and very low-risk areas decreased. The medium risk areas were apparently to be increasing and the high-risk areas were beginning to increase for 50- and 100-year REPs. For 200-year REP, the medium, high, and very high-risk areas increased, and the low and very low-risk areas decreased. Although the high and very high flood risk areas covered the smallest area as compared to other risk classes, they had extreme risk owing to high population

Table 7 Normalization of vulnerability matrix

	LULC	Pop.	DS	$\sum$ of rows	$[E]$	λ_{max}	C_I	C_R
LULC	0.23	0.22	0.33	0.78	3.03	3.039	0.019	0.03
Pop.	0.69	0.65	0.56	1.90	3.07			
DS	0.08	0.13	0.11	0.32	3.01			
$\sum$	1	1	1	3.00	9.11			

Fig. 13 Vulnerability map of the study area

density, medium storm drainage system density, high CN, high drainage density, and very steep slopes.

Figure 15 shows the 145 districts susceptible to flood risk for different REPs. For a 200-year REP, 51% (74 districts) of the area was at very high risk, 24% (35 districts) was at high risk, and 17% (25 districts) was at medium risk of flooding. Only 7% of the area (9 districts) was in a low-risk zone, in addition to 1% (2 districts) in very low-risk areas. Table 9 shows the districts and risk classes for different REPs. For a 2-year REP, the districts had low and very low flood risk. The medium flood risk began to emerge at a 5-year REP. The low and very low-risk areas decreased at the 10-year REP and the medium flood risk increased. For the 25-year REP, the medium risk areas increased and the high-risk areas began to emerge. At a 50-year REP, high-risk areas increased, but the medium risk areas decreased, and the very high areas began to emerge. For 100- and 200-year REPs, the very low, low, and medium flood risk areas decreased and the high and very high flood risk areas increased. The study revealed that factors such as a steeper slope, soil texture, acute precipitation events, and high drainage density

Fig. 14 Flood risk maps for different return periods (REPs)

Table 8 Risk classes percentage area for different return periods (REPs)

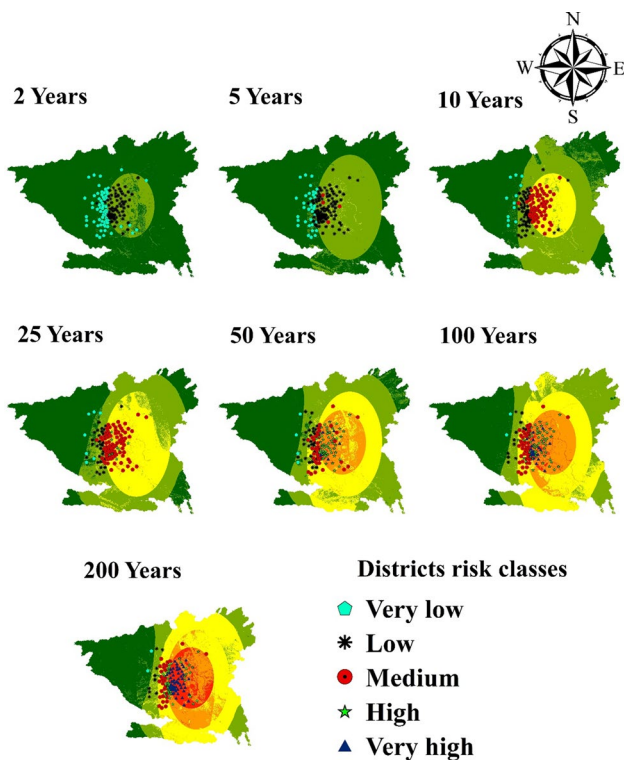| Risk (years)	Very low	Low	Medium	High	Very high
2	87	13	0	0	0
5	65	34	1	0	0
10	46	40	14	0	0
25	36	34	28	2	0
50	29	31	27	12	1
100	25	26	31	15	3
200	24	15	36	14	11

Fig. 15 Risk districts maps for different return periods (REPs)

Table 9 Districts risk class percentage for different return periods (REPs)

Risk (years)	Very low	Low	Medium	High	Very high
2	71 (49%)	74 (51%)	0	0	0
5	35 (24%)	106 (74%)	4 (2%)	0	0
10	12 (9%)	57 (39%)	76 (52%)	0	0
25	7 (4%)	30 (21%)	100 (69%)	8 (6%)	0
50	4 (2%)	27 (19%)	43 (30%)	66 (46%)	5 (3%)
100	2 (1%)	12 (8%)	48 (33%)	59 (41%)	24 (17%)
200	2 (1%)	9 (7%)	25 (17%)	35 (24%)	74 (51%)

aggravate the flood risk. In addition to the aforementioned factors, the effects of uncontrolled urbanization, congested population density, and the inappropriate storm drainage system should also be considered.

Several scientific aspects of flood-prone studies have been highlighted by researchers. Some of them have focused on the physical aspects of analyzing flash floods (Ruin et al. 2008, 2009), while other studies focused on socioeconomic and anthropogenic issues and neglected the physical aspects (Gruntfest and Handmer 2001; Špitalar et al. 2014). One of the studies (Rahman et al. 2016) combined several factors influencing flood vulnerability such as physical, social,

economic, and built-up environmental factors. The present study analyzed different factors influencing flash flood risks (hazard and vulnerability) including socioeconomic, anthropogenic, and physical aspects. The key difference between the studies mentioned above and the current study is that this study considers seven precipitation REPs. Thus, the precipitation intensity alterations during the event besides the likelihood of this event occurring can be thoroughly assessed. Accordingly, this study provides an adequate estimation of the water amount that would accumulate during a potential flooding of the area.

Conclusions

This study focused primarily on flash floods that happen during or after an excessive precipitation event over a very short period. These floods have unforeseen and devastating consequences. Therefore, identifying the vulnerable areas which are possibly at flash floods risk is crucial in mitigating its risks. Consequently, the incorporation of GIS, RST, and spatial AHP was adopted in order that finds the flood risk-prone areas. The flood risk was mapped for the city by amalgamating the hazard and vulnerability maps. The MCE was applied in recognizing the influencing factors the hazard and vulnerability maps. Moreover, the AHP method has been opted to provide weights for every factor. The created Riyadh hazard map has five classes: very low (covering 10% of the city area), low (24%), medium (25%), high (22%), and very high (19%). The vulnerability map also has five classes: very low (covering 25% of the city area), low (15%), medium (26%), high (19%), and very high (15%). The article demonstrates that the risk map can be grouped into five classes for the 100-year precipitation REP. These classes are: very low (covering 25% of the area), low (26%), medium (31%), high (15%), and very high (3%). The flood risk map analysis results show that urban structures, combined with several factors, for instance, extreme rainfall events, gentle slope, high population density, and unplanned urbanization play a significant role in the flood exposure degree.

Riyadh was classified into residential zones, farms, roads, and other infrastructure. The spatial distribution of these features varies from one place to another of the metropolis, alongside the flash flood risk. The high and very high flood risk zones are lying in the heart of the Riyadh metropolitan area. These risks affect urban areas, agricultural lands, roads, barren lands, properties, and infrastructure. For a 100-year REP, more than 57% of the total Riyadh districts were at high and very high flood risk. Moreover, 83 districts out of 145 districts in the city were under high and very high flood risk. Therefore, there is an imperative need to alleviate these risks by structural or non-structural measures. The study will help decision makers in devising potential anticipatory

measures under climate change in mitigating flood risk, harvesting rainwater, and planning controlled urbanization. Additionally, the other studies in the area can, dependable on the method employed in this study.

Compliance with ethical standards

References

Abbas A, Amjath-Babu T, Kächele H, Müller K (2016) Participatory adaptation to climate extremes: an assessment of households' willingness to contribute labor for flood risk mitigation in Pakistan. J Water Clim Chang 7:621–636

Abboud IA, Nofal RA (2017) Morphometric analysis of wadi Khumal basin, western coast of Saudi Arabia, using remote sensing and GIS techniques. J Afr Earth Sci 126:58–74

Abdelkareem M (2017) Targeting flash flood potential areas using remotely sensed data and GIS techniques. Nat Hazards 85:19–37

Ahmad I, Verma V, Verma MK (2015) Application of curve number method for estimation of runoff potential in GIS environment. Paper presented at the 2nd international conference on geological and civil engineering

Aina YA, Merwe J, Alshuwaikhat HM (2008) Urban spatial growth and land use change in Riyadh: comparing spectral angle mapping and band ratioing techniques. Paper presented at the proceedings of the academic track of the 2008 free and open source software for geospatial (FOSS4G) conference, incorporating the GISSA 2008 Conference, Cape Town, South Africa

Amin M, Rizwan M, Alazba A (2016) A best-fit probability distribution for the estimation of rainfall in northern regions of Pakistan Open. Life Sci 11:432–440

Angelakis A (2016) Evolution of rainwater harvesting and use in Crete, Hellas, through the millennia. Water Sci Technol Water Supply 16:1624–1638

Archer D, Fowler H (2018) Characterising flash flood response to intense rainfall and impacts using historical information and gauged data in Britain. J Flood Risk Manag 11:S121–S133

Ashwan MSA, Salam AA, Mouselhy MA (2012) Population growth, structure and distribution in Saudi Arabia. Humanit Soc Sci Rev 1:33–46

Avcioglu B, Anderson CJ, Kalin L (2017) Evaluating the slope-area method to accurately identify stream channel heads in three physiographic regions JAWRA. J Am Water Resour Assoc 53:562–575

Bajabaa S, Masoud M, Al-Amri N (2014) Flash flood hazard mapping based on quantitative hydrology, geomorphology and GIS techniques (case study of Wadi Al Lith, Saudi Arabia). Arab J Geosci 7:2469–2481

Benzougagh B, Dridri A, Boudad L, Kodad O, Sdkaoui D, Bouikbane H (2017) Evaluation of natural hazard of Inaouene watershed river in northeast of Morocco: application of morphometric and geographic information system approaches. Int J Innov Appl Stud 19:85

Cronshey R (1986) Urban hydrology for small watersheds. US Dept. of Agriculture, Soil Conservation Service, Engineering Division

Dale M, Clarke J, Harris H (2016) Urban flood prediction and warning–challenges and solutions. Proc Water Environ Fed 2016:2237–2242. https://doi.org/10.2175/193864716819706022

Danumah JH et al (2016) Flood risk assessment and mapping in Abidjan district using multi-criteria analysis (AHP) model and geoinformation techniques (cote d'ivoire). Geoenviron Disasters 3:1–13

Deng L, McCabe MF, Stenchikov G, Evans JP, Kucera PA (2015) Simulation of flash-flood-producing storm events in Saudi Arabia using the weather research and forecasting model. J Hydrometeorol 16:615–630

Dile YT, Srinivasan R (2014) Evaluation of CFSR climate data for hydrologic prediction in data-scarce watersheds: an application in the Blue Nile River basin JAWRA. J Am Water Resour Assoc 50:1226–1241

Elfeki A, Masoud M, Niyazi B (2017) Integrated rainfall–runoff and flood inundation modeling for flash flood risk assessment under data scarcity in arid regions: Wadi Fatimah basin case study, Saudi Arabia. Nat Hazards 85:87–109

Fisher P, Comber AJ, Wadsworth R (2005) Land use and land cover: contradiction or complement. Re-presenting GIS. Wiley, England, pp 85–98

Fuka DR, Walter MT, MacAlister C, Degaetano AT, Steenhuis TS, Easton ZM (2014) Using the climate forecast system reanalysis as weather input data for watershed models. Hydrol Process 28:5613–5623

Gajbhiye S, Mishra S, Pandey A (2014) Relationship between SCS-CN and sediment yield Applied Water. Science 4:363–370

Gajbhiye S, Mishra S, Pandey A (2015) Simplified sediment yield index model incorporating parameter curve number. Arab J Geosci 8:1993–2004

GhaffarianHoseini A, Tookey J, GhaffarianHoseini A, Yusoff SM, Hassan NB (2016) State of the art of rainwater harvesting systems towards promoting green built environments: a review. Desalin Water Treat 57:95–104

Ghorbani Nejad S, Falah F, Daneshfar M, Haghizadeh A, Rahmati O (2017) Delineation of groundwater potential zones using remote sensing and GIS-based data-driven models. Geocarto Int 32:167–187

Gruntfest E, Handmer J (2001) Dealing with flash floods: contemporary issues and future possibilities. In: Gruntfest E, Handmer J (eds) Coping with flash floods. Springer, Dordrecht, pp 3–10

Hoedjes JC et al (2014) A conceptual flash flood early warning system for Africa, based on terrestrial microwave links and flash flood guidance. ISPRS Int J Geo-Inf 3:584–598

Horton RE (1932) Drainage-basin characteristics Eos. Trans Am Geophys Union 13:350–361

Ibrahim-Bathis K, Ahmed S (2016) Rainfall-runoff modelling of Doddahalla watershed—an application of HEC-HMS and SCN-CN in ungauged agricultural watershed. Arab J Geosci 9:1–16

Karagiorgos K, Thaler T, Hübl J, Maris F, Fuchs S (2016) Multi-vulnerability analysis for flash flood risk management. Nat Hazards 82:63–87

Khan AN (2011) Analysis of flood causes and associated socio-economic damages in the Hindukush region. Nat Hazards 59:1239

Lee RS, Traver RG, Welker AL (2016) Evaluation of soil class proxies for hydrologic performance of in situ bioinfiltration systems. J Sustain Water Built Environ 2:1–10

Li R, Rui X, Zhu A-X, Liu J, Band LE, Song X (2015) Increasing detail of distributed runoff modeling using fuzzy logic in curve number. Environ Earth Sci 73:3197–3205

Mack B, Leinenkugel P, Kuenzer C, Dech S (2017) A semi-automated approach for the generation of a new land use and land cover product for Germany based on Landsat time-series and Lucas in situ data. Remote Sens Lett 8:244–253

Mahmood S, Mayo SM (2016) Exploring underlying causes and assessing damages of 2010 flash flood in the upper zone of Panjkora River. Nat Hazards 83:1213–1227

Mahmood S, Ullah S (2016) Assessment of 2010 flash flood causes and associated damages in Dir Valley, Khyber Pakhtunkhwa Pakistan. Int J Disaster Risk Reduct 16:215–223

Mahmoud SH, Gan TY (2018a) Impact of anthropogenic climate change and human activities on environment and ecosystem services in arid regions. Sci Total Environ 633:1329–1344

Mahmoud SH, Gan TY (2018b) Long-term impact of rapid urbanization on urban climate and human thermal comfort in hot-arid environment. Build Environ 142:83–100

Mahmoud SH, Gan TY (2018c) Multi-criteria approach to develop flood susceptibility maps in arid regions of Middle East. J Clean Prod 196:216–229

Mahmoud SH, Gan TY (2018d) Urbanization and climate change implications in flood risk management: developing an efficient decision support system for flood susceptibility mapping. Sci Total Environ 636:152–167

Mahmoud SH, Gan TY (2019) Irrigation water management in arid regions of Middle East: assessing spatio-temporal variation of actual evapotranspiration through remote sensing techniques and meteorological data. Agric Water Manag 212:35–47

Masoud M (2016) Geoinformatics application for assessing the morphometric characteristics' effect on hydrological response at watershed (case study of Wadi Qanunah, Saudi Arabia). Arab J Geosci 9:1–22

Mishra SK, Singh V (2013) SCS-CN Method. Soil conservation service curve number (SCS-CN) methodology, vol 42. Springer, Dordrecht, pp 84–146

Mohammad FS, Adamowski J (2015) Interfacing the geographic information system, remote sensing, and the soil conservation service–curve number method to estimate curve number and runoff volume in the Asir region of Saudi Arabia. Arab J Geosci 8:11093–11105

Mohan T, Rajeevan M (2017) Past and future trends of hydroclimatic intensity over the Indian Monsoon region. J Geophys Res Atmosp 122:896–909

NRCS (2007) National engineering handbook: part 630—hydrology, USDA Soil Conservation Service. Washington, DC, USA. https://directives.sc.egov.usda.gov/viewerFS.aspx?hid=21422. Accessed 22 Mar 2017

NRCS (2009) National engineering handbook: part 630—hydrology, USDA Soil Conservation Service. Washington, DC, USA. https://directives.sc.egov.usda.gov/viewerFS.aspx?hid=21422. Accessed 22 Mar 2017

Oliveira P, Nearing M, Hawkins R, Stone J, Rodrigues D, Panachuki E, Wendland E (2016) Curve number estimation from Brazilian Cerrado rainfall and runoff data. J Soil Water Conserv 71:420–429

Ouma YO, Tateishi R (2014) Urban flood vulnerability and risk mapping using integrated multi-parametric AHP and GIS: methodological overview and case study assessment. Water 6:1515–1545

Papaioannou G, Vasiliades L, Loukas A (2015) Multi-criteria analysis framework for potential flood prone areas mapping. Water Resour Manag 29:399–418

Qhtani AM, Al Fassam AN (2011) Ar Riyadh Geospatial urban information system and metropolitan development strategy for Ar Riyadh. Paper presented at the ESRI international user conference

Radwan F, Alazba A, Mossad A (2017) Watershed morphometric analysis of Wadi Baish Dam catchment area using integrated GIS-based approach. Arab J Geosci 10:256

Rahman MT, Aldosary AS, Nahiduzzaman KM, Reza I (2016) Vulnerability of flash flooding in Riyadh, Saudi Arabia. Nat Hazards 84:1807–1830

Rahmati O, Zeinivand H, Besharat M (2016) Flood hazard zoning in Yasooj region, Iran, using GIS and multi-criteria decision analysis. Geomat Nat Hazards Risk 7:1000–1017

Rai PK, Mohan K, Mishra S, Ahmad A, Mishra VN (2017) A GIS-based approach in drainage morphometric analysis of Kanhar River Basin, India. Appl Water Sci 7:217–232

Ranjan R (2017) Flood disaster management. In: Sharma N (ed) River system analysis and management. Springer, Singapore, pp 371–417

Redwan M, Rammlmair D (2017) Flood hazard assessment and heavy metal distributions around Um Gheig mine area, Eastern Desert, Egypt. J Geochem Explor 173:64–75

Rimba AB, Setiawati MD, Sambah AB, Miura F (2017) Physical flood vulnerability mapping applying geospatial techniques in Okazaki City, Aichi Prefecture, Japan. Urban Sci 1:1–22

Ruin I, Creutin J-D, Anquetin S, Lutoff C (2008) Human exposure to flash floods—relation between flood parameters and human vulnerability during a storm of September 2002 in Southern France. J Hydrol 361:199–213

Ruin I, Creutin J-D, Anquetin S, Gruntfest E, Lutoff C (2009) Human vulnerability to flash floods: addressing physical exposure and behavioural questions. Paper presented at the Flood risk management: research and practice proceedings of the European Conference on Flood Risk Management Research into Practice (FLOODrisk 2008), Oxford, UK, 30 September-2 October 2008

Ryu J, Jung Y, Kong DS, Park BK, Kim YS, Engel BA, Lim KJ (2016) Approach of land cover based asymptotic curve number regression equation to estimate runoff. Irrig Drain 65:94–104

Saaty TL (1980) The analytical hierarchy process: planning, priority setting, resource allocation. RWS publication, Pittsburg

Sartori A, Hawkins RH, Genovez AM (2011) Reference curve numbers and behavior for sugarcane on highly weathered tropical soils. J Irrig Drain Eng 137:705–711

Shadeed S, Almasri M (2010) Application of GIS-based SCS-CN method in West Bank catchments. Palest Water Sci Eng 3:1–13

Špitalar M, Gourley JJ, Lutoff C, Kirstetter P-E, Brilly M, Carr N (2014) Analysis of flash flood parameters and human impacts in the US from 2006 to 2012. J Hydrol 519:863–870

Starosolszky O, Melder O (2014) Hydrology of disasters: proceedings of the world meteorological organization technical conference held in Geneva, November 1988. Routledge

Stefanidis S, Stathis D (2013) Assessment of flood hazard based on natural and anthropogenic factors using analytic hierarchy process (AHP). Nat Hazards 68:569–585

Subyani AM, Al-Amri NS (2015) IDF curves and daily rainfall generation for Al-Madinah city, western Saudi Arabia. Arab J Geosci 8:11107–11119

Tirkey AS, Ghosh M, Pandey A, Shekhar S (2017) Assessment of climate extremes and its long term spatial variability over the Jharkhand state of India. Egypt J Remote Sens Space Sci 21:49–63

Wu M, Che Y, Lv Y, Yang K (2017) Neighbourhood-scale urban riparian ecosystem classification. Ecol Indic 72:330–339

Yalcin M, Gul FK (2017) A GIS-based multi criteria decision analysis approach for exploring geothermal resources: Akarcay basin (Afyonkarahisar). Geothermics 67:18–28

Zhang Q, Luo G, Li L, Zhang M, Lv N, Wang X (2017) An analysis of oasis evolution based on land use and land cover change: a case study in the Sangong River Basin on the northern slope of the Tianshan Mountains. J Geog Sci 27:223–239